First principles phase diagram calculations for the wurtzite-structure systems AlN–GaN, GaN–InN, and AlN–InN

B. P. Burton[a)]
Ceramics Division, Materials Science and Engineering Laboratory, National Institute of Standards and Technology, Gaithersburg, Maryland 20899-8520

A. van de Walle[b)]
Materials Science and Engineering Department, Northwestern University, 2225 North Campus Drive, Evanston, Illinois 60208

U. Kattner
Metallurgy Division, Materials Science and Engineering Laboratory, National Institute of Standards and Technology, Gaithersburg, Maryland 20899-8520

(Received 7 February 2006; accepted 14 September 2006; published online 13 December 2006)

First principles phase diagram calculations were performed for the wurtzite-structure quasibinary systems AlN–GaN, GaN–InN, and AlN–InN. Cluster expansion Hamiltonians that excluded, and included, excess vibrational contributions to the free energy, F_{vib}, were evaluated. Miscibility gaps are predicted for all three quasibinaries, with consolute points, (X_C, T_C), for AlN–GaN, GaN–InN, and AlN–InN equal to (0.50, 305 K), (0.50, 1850 K), and (0.50, 2830 K) without F_{vib}, and (0.40, 247 K), (0.50, 1620 K), and (0.50, 2600 K) with F_{vib}, respectively. In spite of the very different ionic radii of Al, Ga, and In, the GaN–InN and AlN–GaN diagrams are predicted to be approximately symmetric. © *2006 American Institute of Physics*. [DOI: 10.1063/1.2372309]

I. INTRODUCTION

Because of their wide direct band gaps,[1] wurtzite-structure AlN [6.28 eV (Ref. 2)], GaN [3.5 eV (Ref. 3)], and InN [1.89 eV (Ref. 4), and 0.7 eV (Ref. 5)] are widely used to make light emitting diodes, laser diodes, and a variety of other optoelectronic devices.[6–9] Alloying is used to tune band gaps for desired wavelengths of emitted light, but unmixing in GaN–InN and AlN–InN (Refs. 10–13) limits the range of homogeneous alloys that can be synthesized, and therefore the accessible range of emitted colors. This problem stimulated interest in the mixing properties of all three systems, but to date, none of the equilibrium quasibinary phase diagrams has been determined experimentally, either for bulk samples or for thin films.

Since the early 1990s, there have been many computational and experimental investigations of excess vibrational entropy, F_{vib},[14] and its effects on the phase stabilities of intermetallics and alloys, e.g., Refs. 15–18 and the review[19] which tabulates 19 systems that were modeled computationally and 16 that were studied experimentally. In a system with a miscibility gap, including F_{vib} in a first principles phase diagram (FPPD) calculation typically leads to a modest percentage reduction in the consolute temperature T_C:[20]

$$5\,\% \lesssim \%\,\Delta T_C \lesssim 15\% \tag{1.1}$$

$$\%\Delta T_C \equiv 200(T_C - T_C^{\mathrm{vib}})/(T_C + T_C^{\mathrm{vib}}), \tag{1.2}$$

where T_C is the FPPD value without F_{vib}, and T_C^{vib} is the FPPD value with F_{vib}. A striking exception is the system NaCl–KCl,[21] in which the T_C reduction approaches 50%. The systems AlN–GaN, GaN–InN, and AlN–InN constitute a convenient, structurally homologous set for examining the importance of F_{vib} as a function of T_C or as a function of difference in ionic size.

Empirical valence force field (VFF) calculations for wurtzite-structure solid solutions[22,23] predict miscibility gaps with consolute temperatures T_C of 171 K for AlN–GaN, 1668 K for GaN–InN, and 3399 K for AlN–InN. Takayama *et al.*[22,23] also report $T_C = 1676$ K and $T_C = 1678$ K for GaN–InN in the ideal wurtzite and zinc blende structures, respectively, and Adhikari and Kofke[24] reports $T_C = 1678$ K, for zinc blende structure GaN–InN. These calculations combine VFF formulations of the excess enthalpy with strictly regular solution models, a methodology that has two serious limitations: (1) it necessarily yields symmetric miscibility gaps with $X_C = 0.5$, and (2) ignores clustering (short-range order) and therefore a potentially significant contribution to the configurational entropy.

Typically, miscibility gaps between end member compounds with ions that have very different ionic radii, R_i, are asymmetric with reduced solubility on the side of the diagram corresponding to the smaller exchangeable ion and enhanced solubility on the other. For example, in the NaCl–KCl phase diagram, the consolute point is $\{X_C, T_C\} = \{0.348, 765\ \mathrm{K}\}$,[26,27] where X_C is the consolute composition in units of mole fraction (X) KCl. The percentage differences in ionic radii,

$$\%\,\Delta R_{ij} = 200|R_i - R_j|/(R_i + R_j), \tag{1.3}$$

for NaCl–KCl and the III-V nitride systems are $\%\Delta R_{\mathrm{Na,K}} = 26.9$, $\%\Delta R_{\mathrm{Al,Ga}} = 14.0$, $\%\Delta R_{\mathrm{Ga,In}} = 23.6$, and $\%\Delta R_{\mathrm{Al,In}} = 35.7$, ($R_{\mathrm{Na}}^{\mathrm{VI}} = 1.16$ Å, $R_{\mathrm{K}}^{\mathrm{VI}} = 1.52$ Å, $R_{\mathrm{Al}}^{\mathrm{IV}} = 0.53$ Å, $R_{\mathrm{Ga}}^{\mathrm{IV}} = 0.61$ Å, and $R_{\mathrm{In}}^{\mathrm{IV}} = 0.76$ Å;[25] Roman numerals indicate coor-

a)Electronic mail: benjamin.burton@nist.gov
b)Electronic mail: avdw@northwestern.edu

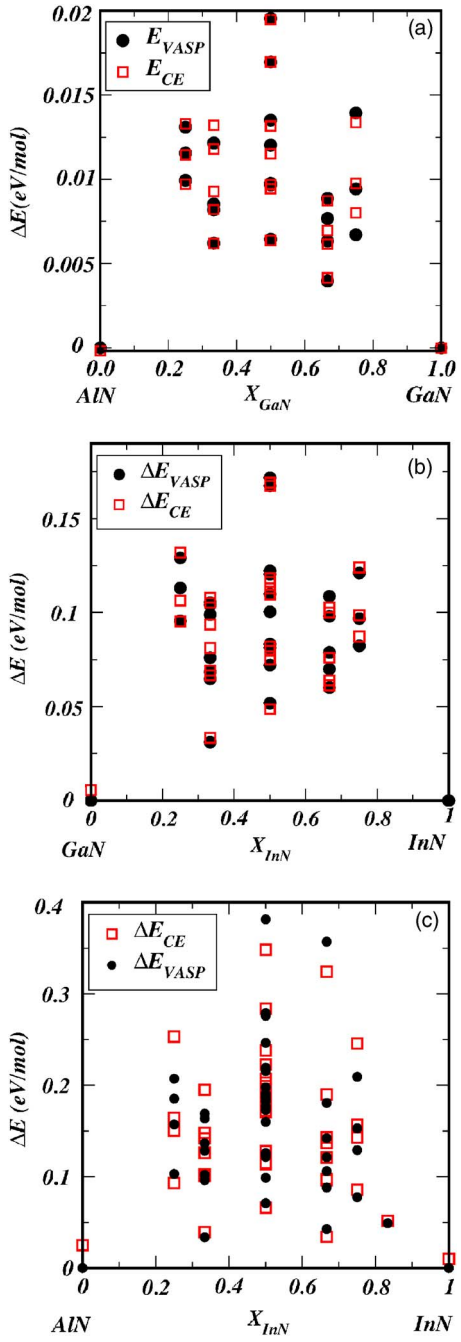

FIG. 1. (Color online) Formation energies, ΔE_f, for (a) $Al_{1-x}Ga_xN$, (b) $Ga_{1-x}In_xN$, and (c) $Al_{1-x}In_xN$ supercells. The closed circles are VASP results, and the open squares are values calculated with cluster expansion Hamiltonians that were fitted to 0 K VASP results. All $\Delta E_f > 0$ indicating misciblilty gaps in all three systems, at least in the neighborhood of 0 K.

dination numbers). Thus one might reasonably expect less asymmetry in GaN–InN than in NaCl–KCl, $0.348 < X_C < 0.5$, and more in AlN–InN, $X_C < 0.348$. Surprisingly, however, the FPPD results reported here predict symmetrical diagrams for both GaN–InN and AlN–InN.

II. COMPUTATIONAL METHODS

Formation energies, ΔE_f (Figs. 1) were calculated for wurtzite-structure AlN, GaN, and InN and many

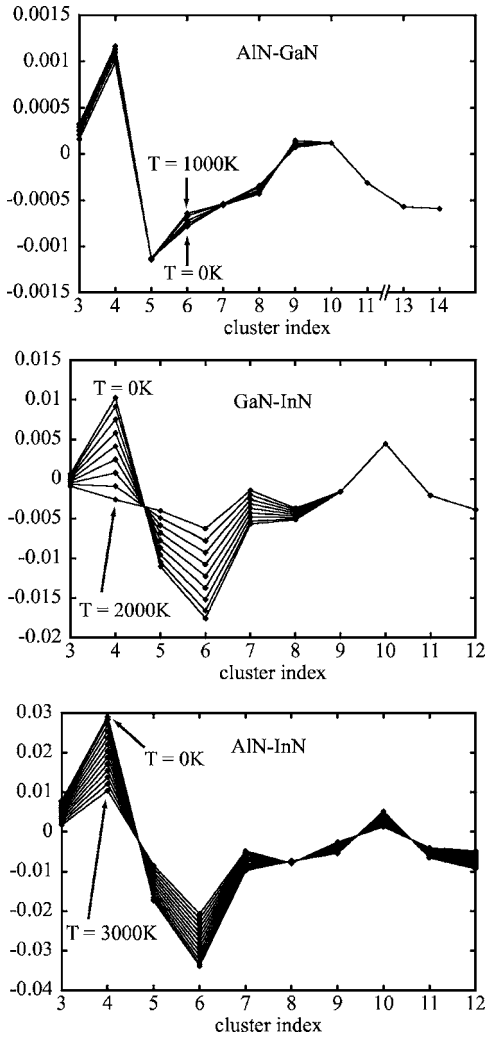

FIG. 2. Temperature dependence of the effective cluster interactions. The interactions are given at intervals of 250 K from 0 K to a temperature lying above the miscibility gap for the corresponding system. In all cases, larger interactions (in absolute value) correspond to lower temperatures. The cluster index refers to the clusters given in Table II.

$M_mM'_nN_{(m+n)}$ supercells, in which M and M' are Al, Ga, or In. All electronic structure calculations were performed with the Vienna *ab initio* simulation program (VASP,[28]) using ultrasoft Vanderbilt-type plane-wave pseudopotentials[29] with the generalized gradient approximation (GGA) for exchange and correlation energies. Electronic degrees of freedom were optimized with a conjugate gradient algorithm, and both cell constant and ionic positions were fully relaxed. Valence electron configurations for the pseudopotentials are Al_h $2s^13p^1$, Ga_d $4s^23d^{10}4p^1$, In_d $5s^25p^1$, and N_s $2s^22p^3$. Total energy calculations were converged with respect to k-point meshes, and an energy cutoff of 400 eV was used, in the "high precision" option which yields ΔE_f values that are converged to within a few meV per exchangeable cation (Al, Ga, In).

Remaining steps of the FPPD calculations were performed with the ATAT software package.[19(b)–19(d)] First, VASP calculations were used to construct cluster expansion (CE) Hamiltonians,[30] in which optimal cluster sets were determined by minimizing the cross-validation score.[19(b)] The effective cluster interactions (ECIs) which define the CE are

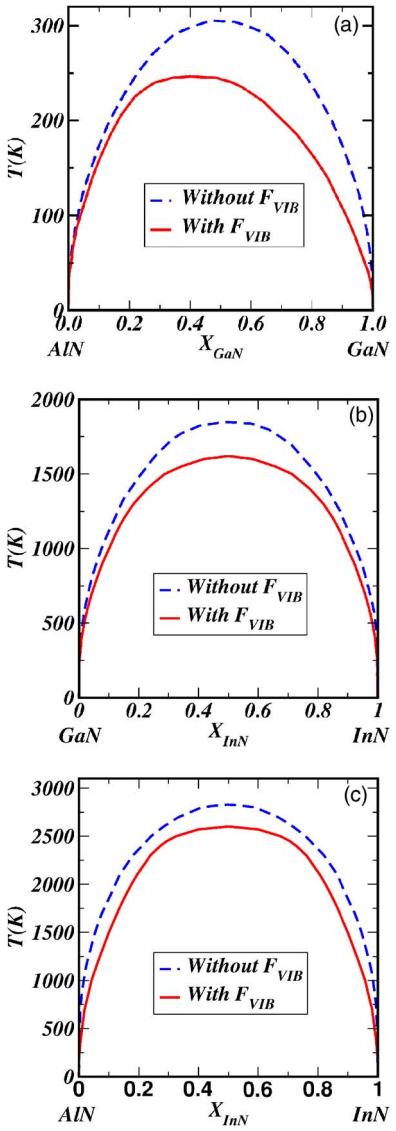

FIG. 3. (Color online) Calculated phase diagrams for the systems (a) AlN–GaN, (b) GaN–InN, and (c) AlN–InN. The dashed (blue) curves are for calculations that did not include F_{vib}, and the solid (red) curves are for calculations that did.

obtained by a least-squares fit to the VASP energies.

Contributions of lattice vibrations to the free energies were included via the coarse-graining formalism.[19(a)] The vibrational free energy (F_{vib}) as a function of temperature was calculated in the harmonic approximation for each of the superstructures included in the CE fit. The quantum mechanical expression for the free energy was used, rather than the more usual high-temperature, or classical, limit. To reduce the computational burden of obtaining phonon densities of states for a large set of superstructures, the bond-length-dependent transferable force constant scheme[19(a)] was employed. As discussed/justified in Ref. 21, nearest-neighbor force constants were obtained for high-symmetry structures (the end members AlN, GaN, and InN) as functions of imposed lattice parameters, i.e., bond lengths. The resulting bond stiffness versus. bond length relationships were then used to predict force constants for all remaining superstructures, using the relaxed bond lengths and the chemical identities of bonds as predictors of their stiffnesses. Resulting free energies were then used to fit temperature-dependent CE V, which were used as input for grand-canonical Monte Carlo simulations, to calculate phase diagrams.

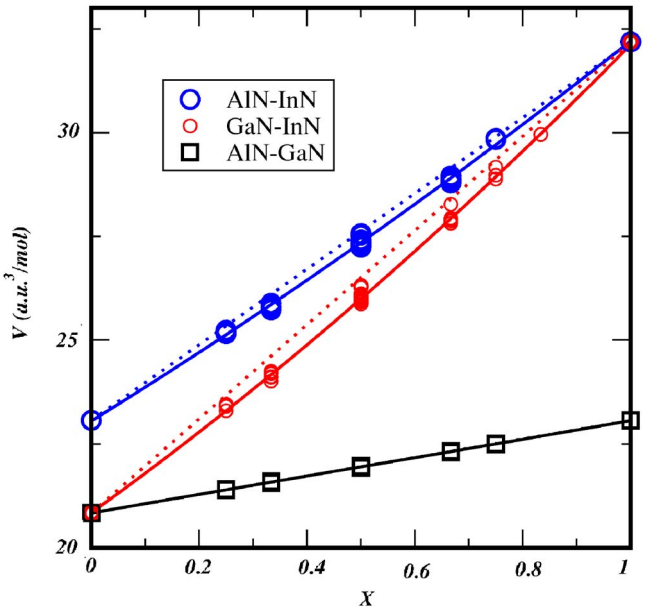

FIG. 4. (Color online) Cluster expansion fits (solid lines), and VASP supercell calculations (open circles and squares), of molar volume as functions of composition for the systems AlN–GaN, GaN–InN, and AlN–InN. The dashed lines connect end points for the supercell calculations.

III. RESULTS AND DISCUSSION

Figures 1 depict the databases of 0 K *ab initio* formation energies, $\{\Delta E_f\}$, that were used in the CE Hamiltonian fits, and the corresponding predicted energies from the resulting CEs. Table I reports the bond-length-dependent force constants determined from supercell calculations and used to calculate vibrational contributions to the free energy, F_{vib}. The ECIs of the CE Hamiltonians are listed in Table II, in which the superscripts T indicate interactions that are temperature dependent in the FPPD calculations which include F_{vib}. The criterion for selecting the subset of ECIs that are T dependent is minimization of the cross-validation score for the fit to the set $\{F_{vib}\}$; this selection was made in the limit of

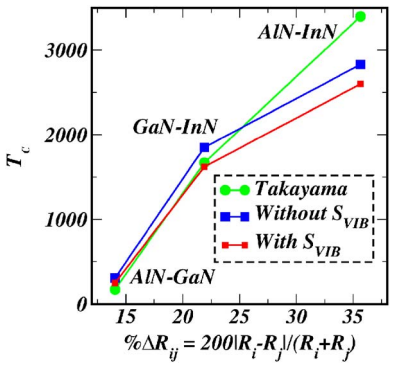

FIG. 5. (Color online) Variation of T_C as a function of the percentage difference in the ionic radii of exchangeable ions. As expected T_C correlates with the difference in ionic radii.

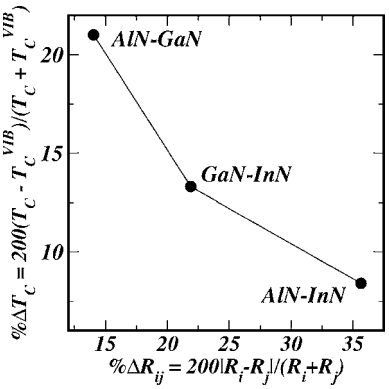

FIG. 6. Percentage reduction in the calculated values of T_C that are induced by including F_{vib} in the cluster expansion Hamiltonian, plotted as functions of the percentage difference in the ionic radii of exchangeable cations. Clearly, the importance of F_{vib} anticorrelates with T_C.

high temperature, and the same subset was used at all temperatures. Figure 2 plots the T-dependent ECIs for each system. In all cases, ECI magnitudes decrease with temperature. These are harmonic approximation results, but the effects of thermal expansion on F_{vib} are negligible in these systems. Differences between the quasiharmonic and harmonic free energies were typically of the order of 4×10^{-5} eV/at. and never exceeded 2×10^{-4}eV/at., which is small relative to the scale of the harmonic contributions ($\sim10^{-3}$eV/at.) to the free energies of formation.

The FPPD results for CE Hamiltonians that exclude F_{vib}, Table II, are represented by the dashed (blue) curves in Figs. 3. The FPPD miscibility gaps from CEs that include F_{vib} are represented by solid (red) curves in Figs. 3. Calculated values for consolute points, $\{X_C, T_C\}$, are listed in Table III, where they are compared to the VFF results of Takayama *et al.*[22,23]

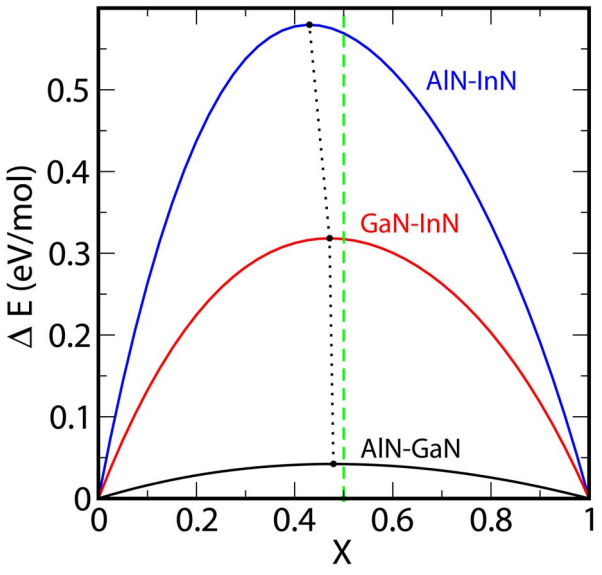

FIG. 7. (Color online) Zero pressure $\Delta E(X)$ $\Delta H(X)$ curves estimated by the $\epsilon-G$ approximation. (Ref. 34). The dotted line connecting maxima indicates a prediction of monotonically increasing asymmetry in the strain energy for the sequence AlN–GaN, GaN–InN, and AlN–InN.

TABLE I. Bond-length-dependent transferable force constants.

Bond type	Force constant type (s: stretching, b: bending)	Constant (eV/Å^2)	Length dependence (eV/Å^3)
Al–N	s	283.2	−143.6
	b	−64.2	35.2
Ga–N	s	164.1	−79.7
	b	−34.1	18.4
In–N	s	135.0	−58.5
	b	−28.8	13.7

To facilitate calculation of phase diagrams (CALPHAD)-type[31] modeling, Redlich-Kister polynomial representations of the Gibbs energy were fitted to the FPPD phase boundaries (Figs. 3), and the resulting coefficients are listed in Table IV. For these fits, the wurtzite structure was described with a two-sublattice model, $(M,M')_1(N)_1$, in which M,M'=Al, Ga, In:

$$G^{\text{ex}} = y_1 y_2 \sum_{i=0}^{2} (y_1 - y_2)^i (H_i - S_i T). \tag{3.1}$$

Here y_1 and y_2 are site fractions of M and M', respectively. Descriptions as regular or quasiregular solutions were not sufficient to reproduce the FPPD phase boundaries: miscibility gap widths at lower temperatures were overestimated; and asymmetry in the AlN–GaN gap was not reproduced. Therefore, higher order polynomials were fitted.

The absence of three-body or other odd-order terms in the CE Hamiltonians for GaN–InN and AlN–InN (Table II) implies that the FPPD calculations for these systems necessarily yield symmetric phase diagrams with X_C=0.5. This result reflects the approximate equalities of ΔE_f values for complementary supercells, i.e., supercell ordered configurations that are related by cation species interchange, e.g., $AlGa_3N_4$ and Al_3GaN_4 supercells with identical crystal structures. More formally, if the formation energy of structure s is $\Delta E_f(s)$ and ΔE_f for its complimentary structure is $\Delta E_f(s_c)$, then the absence of odd-order terms in the CEs implies that the approximation $\Delta E_f(s)=E_f(s_c)$ yields the best overall CE fits for GaN–InN and AlN–InN. Note that the map code uses a cross-validation score analysis to select the optimum CE. Therefore, the absence of odd-order terms is aprediction, not a choice, or an implicit assumption, whereas it is a choice in the VFF plus strictly regular solution model approach.[22,23]

Cluster expansions of molar volumes as functions of bulk composition are plotted in Fig. 4; where 1 mole equals a mole of exchangeable cations. In Fig. 4, the dashed lines indicate linear trends between end members, the symbols (circles and squares) indicate VASP supercell volumes, and the solid curves indicate CE fits to the complete structure sets. Trends for all three systems are close to linear with a fit for AlN–GaN that is within computational error of linear; small but significant negative nonlinearities in GaN–InN (V =23.0512+8.042 52X+1.113 83X^2) and AlN–InN (V =20.8388+9.345 85X+1.935 18X^2).

TABLE II. Effective cluster interactions.

Index	Cluster coordinates	$d_{i,j}$[a] (Å) (eV/cation)	AlN–GaN ECI (eV/cation)	GaN–InN ECI (eV/cation)	AlN–InN ECI
1	Zero cluster		0.023 515	0.022 812	0.326 036
2	Point cluster		−0.001 597	0.078 193	−0.007 548
3	(2/3, 1/3, 1) (1/3, −1/3, 3/5)	3.07	$-0.000\ 160^{T}$[b]	$0.000\ 720^{T}$	$0.008\ 358^{T}$
4	(2/3, 1/3, 1) (5/3, 1/3, 1)	3.11	$0.001\ 697^{T}$	$0.010\ 966^{T}$	$0.030\ 861^{T}$
5	(1/3, 2/3, 1/2) (−1/3, 4/3, 0)	4.37	$-0.001\ 229^{T}$	$-0.011\ 463^{T}$	$-0.018\ 402^{T}$
6	(1/3, 2/3, 1/2) (1/3, 2/3, −1/2)	4.98	$-0.002\ 217^{T}$	$-0.018\ 280^{T}$	$-0.035\ 087^{T}$
7	(1/3, 2/3, 1/2) (2/3, 7/3, 0)	5.36	$-0.000\ 617^{T}$	$-0.005\ 989^{T}$	$-0.010\ 349^{T}$
8	(1/3, 2/3, 1/2) (4/3, −1/3, 1/2)	5.39	$-0.000\ 809^{T}$	$-0.005\ 278^{T}$	$-0.007\ 647^{T}$
9	(1/3, 2/3, 1/2) (1/3, −1/3, −1/2)	5.87	−0.000 236	$-0.001\ 612^{T}$	$-0.005\ 833^{T}$
10	(1/3, 2/3, 1/2) (1/3, −4/3, 1/2)	6.22	−0.000 366	$-0.004\ 466^{T}$	$-0.005\ 576^{T}$
11	(1/3, 2/3, 1/2) (−4/3, 4/3, 0)	6.94	−0.000 320	$-0.002\ 096^{T}$	$-0.006\ 792^{T}$
12	(2/3, 1/3, 1) (−1/3, 4/3, 0)	7.34		$-0.003\ 852^{T}$	$-0.009\ 581^{T}$
13	(2/3, 1/3, 1) (4/3, 2/3, 1/2) (5/3, 1/3, 1)	3.11	$0.000\ 446^{T}$		
14	(2/3, 1/3, 1) (2/3, −2/3, 1) (5/3, 1/3, 1)	3.11	0.000 341		
	Cross-validation scores[c]		0.001 27 0.083 1	0.009 50 0.050 9	0.039 97 0.054 6

[a] $d_{i,j}$ is the longest pair distance within the cluster.
[b] Superscript T indicates an effective cluster interaction that is temperature dependent when F_{vib} is included in the effective Hamiltonian.
[c] First row is the CV score without T-dependent ECIs, and second row is the CV score with T-dependent ECIs.

Figure 5 is a plot of T_C as a function of the percentage difference between the ionic radii of exchangeable cations, $\%\Delta R_{ij}=200|R_i-R_j|/(R_i+R_j)$. As expected, T_C is positively correlated with $\%\Delta R_{ij}$, supporting the presumption that immiscibility in these systems is driven by an ionic size effect. Results of the VFF calculations (large circles) are also plotted in Fig. 5. Percentage differences in calculated T_C's, between the VFF and FPPD calculations with F_{vib} included, are 30.8%, 19.3%, and 26.6% for AlN–GaN, GaN–InN, and AlN–InN, respectively. Because the VFF calculations ignore clustering (short-range order) they necessarily predict higher T_C's than they would if it were included, i.e., if the energetics that drive immiscibility have any short-range character, then T_C's are systematically overestimated in the VFF calculations.

TABLE III. Calculated consolute points.

System	Without F_{vib} $\{X_C, T_C\ (K)\}$	With F_{vib} $\{X_C, T_C\ (K)\}$	Method reference
AlN–GaN	0.48(2), 305(5)	0.40(2), 247(5)	FPPD[a]
	0.50, 181		VFF[b]
GaN–InN	0.50, 1850(10)	0.50, 1620(10)	FPPD[a]
	0.50, 1967		VFF[b]
AlN–InN	0.50, 2830(10)	0.50, 2600(10)	FPPD[a]
	0.50, 3399		VFF[b]

[a] FPPD=first principles phase diagram, this work.
[b] VFF=valence force field, (Refs. 22 and 23); these calculations use a strictly regular solution model which implies symmetrical phase diagrams with $X_C=0.5$. Numbers in parentheses indicate approximate errors in the last digit(s).

As noted above, including F_{vib} typically leads to a 5%–15% reduction in the calculated value for T_C, and calculated results for GaN–InN and AlN–InN are within this range, Fig. 5. Clearly, Fig. 6, $\%\Delta T_C$ is anticorrelated with $\%\Delta R_{i,j}$, and therefore anticorrelated with T_C as well. Thus, within this structurally homologous set of systems, the relative contributions of the vibrational free energy F_{vib} increase monotonically as T_C decreases. The most interesting results of these calculations are the predictions of symmetrical phase diagrams for GaN–InN and AlN–InN. As noted above, one expects an asymmetric diagram when ions of different sizes are mixed in a solid solution. These systematics can be rationalized in terms of a pair potential bonding model. Pair poten-

TABLE IV. Coefficients of Redlich-Kister polynomial representations of the Gibbs energies that were fitted to FPPD phase boundaries.

	(Al,Ga)N		(Ga,In)N		(Al,In)N	
Polynomial terms	H	S	H	S	H	S
$y_1\ y_2$	4180.0	6.666 95	263 81.4	2.139 41	43 766.9	2.402 91
$y_1\ y_2\ (y_1-y_2)$	0	−5.953 24	0	0	0	0
$y_1\ y_2\ (y_1-y_2)^2$	−986.5	1.811 64	−434 5.5	0.126 46	−4 128.2	1.178 19
Consolute points	T (K)	y_2	T (K)	y_2	T (K)	y_2
Subregular (H only)	311	0.5	1 848	0.5	2 880	0.5
Quasisubregular (H, S)	259	0.43	1 648	0.5	2 683	0.5

tials are asymmetric such that compression costs more energy than expansion, and therefore it takes more energy to replace a smaller ion with a larger one than vice versa. Hence there is enhanced solubility on the side of the phase diagram corresponding to the larger ion. A similar conclusion obtains when the elastic energy that drives immiscibility is formulated from end member equations of state, (EOSs) as in the ϵ-G approximation,[32–35] in which the elastic energy is approximated by (1) calculating EOS for end members, (2) approximating $V=V(X)$ as linear (Vegard's law) or with a CE fitted curve such as those plotted in Fig. 7, and (3) approximating $\Delta E(X)$ as a linear combination of partials from the end member EOS. This procedure with $V(X)$ from the CE curves in Fig. 4 was used to generate the $\Delta E(X)$ curves plotted in Fig. 7. All three curves have the expected characteristic asymmetry, with maxima closer to the end member corresponding to the smaller ion.

It is unclear why the calculated formation energies for GaN–InN and AlN–InN have approximate symmetry with respect to species exchange. It seems likely that this surprising result reflects unusual strain accommodation in the wurtzite structure.

IV. CONCLUSIONS

For the AlN–GaN, GaN–InN, and AlN–InN systems, respectively: (1) FPPD calculations predict miscibility gaps with consolute temperatures T_C of 247, 1620, and 2600 K, and (2) the percentage reductions in calculated consolute temperatures T_C induced by the inclusion of vibrational contributions to the free energy are −30.8%, 19.3%, and 26.6%. Surprisingly, the GaN–InN and AlN–InN FPPD phase diagrams are predicted to be approximately symmetric; this is in contrast to the VFF calculations of Takayama *et al.*[22,23] in which symmetric phase diagrams are assumed at the outset.

[1] B. T. Liou, S.-H. Yen, and Y.-K. Kuo, Appl. Phys. A: Mater. Sci. Process. **81**, 1459 (2005).
[2] P. B. Perry and R. F. Rutz, Appl. Phys. Lett. **33**, 319 (1978).
[3] B. Monemar, Phys. Rev. B **10**, 676 (1974).
[4] T. L. Tanesley and C. P. Foley, J. Appl. Phys. **59**, 3241 (1986).
[5] V. Yu. Davydov *et al.*, Phys. Status Solidi B **234**, 787 (2002); **229**, R1 (2002).
[6] S. J. Pearton, J. C. Zolper, R. J. Shul, and F. Ren, J. Appl. Phys. **86**, 1 (1999).
[7] S. C. Jain, M. Willander, J. Narayan, and R. Van Overstraeten, J. Appl. Phys. **87**, 965 (2000).
[8] T. Mukai *et al.*, Phys. Status Solidi A **200**, 52 (2003).
[9] M. A. Khan, M. Shatalov, H. P. Maruska, H. M. Wang, and E. Kuokstis, Jpn. J. Appl. Phys., Part 1 **44**, 7197 (2005).
[10] R. Singh, D. Doppalapudi, and T. D. Moustakas, Appl. Phys. Lett. **70**, 1089 (1997).
[11] A. Wakahara, T. Tokuda, X.-Z. Dang, S. Noda, and A. Sasaki, Appl. Phys. Lett. **71**, 906 (1997).
[12] Y.-S. Lin *et al.*, Appl. Phys. Lett. **77**, 2988 (2000).
[13] S.-W. Feng *et al.*, Appl. Phys. Lett. **83**, 3906 (2003).
[14] Excess with respect to the vibrational entropy of a mechanical mixture of end members with the same bulk composition.
[15] G. D. Garbulsky and G. Ceder, Phys. Rev. B **49**, 6327 (1994); **53**, 8993 (1996).
[16] S. Silverman, A. Zunger, R. Kalish, and J. Adler, J. Phys.: Condens. Matter **7**, 1167 (1995); Phys. Rev. B **51**, 10795 (1995).
[17] L. Anthony, J. K. Okamoto, and B. Fultz, Phys. Rev. Lett. **70**, 1128 (1993).
[18] L. Anthony, L. J. Nagel, J. K. Okamoto, and B. Fultz, Phys. Rev. Lett. **73**, 3034 (1994).
[19] A. van de Walle and G. Ceder, Rev. Mod. Phys. **74**, 11 (2002); J. Phase Equilib. **23**, 348 (2002); A. van de Walle, M. Asta, and G. Ceder, CALPHAD: Comput. Coupling Phase Diagrams Thermochem. **26**, 539 (2002); A. van de Walle and M. Asta, Modell. Simul. Mater. Sci. Eng. **10**, 521 (2002).
[20] The consolute temperature T_C is the maximum temperature of the miscibility gap.
[21] B. P. Burton and A. van de Walle, Chem. Geol. **225** [3–4], 222 (2006).
[22] T. Takayama, M. Yuri, K. Itoh, B. Takaaki, and J. S. Harris, Jr., Jpn. J. Appl. Phys., Part 1 **39**, 5057 (2000).
[23] T. Takayama, M. Yuri, K. Itoh, and J. S. Harris, Jr., Jpn. J. Appl. Phys., Part 1 **90**, 2358 (2001).
[24] J. Adhikari and D. A. Kofke, J. Appl. Phys. **95**, 6129 (2004).
[25] http://www.webelements. com/webelements/elements/text/H/radii.html
[26] J. B. Thompson and D. R. Waldbaum, Geochim. Cosmochim. Acta **33**, 671 (1969).
[27] D. Walker, P. K. Verma, L. M. D. Cranswick, S. M. Clark, R. L. Jones, and S. Bure, Am. Mineral. **90**, 229 (2005).
[28] G. Kresse and J. Hafner, Phys. Rev. B **47**, 558 (1993); G. Kresse, thesis, Technische Universität Wien, 1993; Phys. Rev. B **49**, 14251 (1994); G. Kresse and J. Furthmüller, Comput. Mater. Sci. **6**, 15 (1996); Phys. Rev. B **54**, 11169 (1996); cf. http://tph.tuwien.ac.at/vasp/guide/vasp.html
[29] D. Vanderbilt, Phys. Rev. B **41**, 7892 (1990).
[30] J. M. Sanchez, F. Ducastelle, and D. Gratias, Physica A **128**, 334 (1984).
[31] U. R. Kattner, JOM **49**, 14 (1997).
[32] L. G. Ferriera, A. A. Mbaye, and A. Zunger, Phys. Rev. B **35**, 6475 (1987).
[33] A. Zunger, S.-H. Wei, A. A. Mbaye, and L. G. Ferriera, Acta Metall. **36**, 2239 (1987).
[34] L. G. Ferriera, A. A. Mbaye, and A. Zunger, Phys. Rev. B **37**, 10547 (1988).
[35] B. P. Burton, N. Dupin, S. G. Fries, G. Grimvall, A. Fernández Guillermet, P. Miodownik, W. A. Oats, and V. Vinograd, Z. Metallkd. **92**, 514 (2001).